Aging Brain 5 (2024) 100103

Contents lists available at ScienceDirect

Aging Brain

journal homepage: www.elsevier.com/locate/nbas

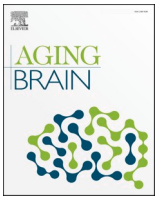

Grey-matter structure in cortical and limbic regions correlates with general cognitive ability in old age

Ylva Köhncke [a], Simone Kühn [b,c], Sandra Düzel [a], Myriam C. Sander [a], Andreas M. Brandmaier [a,d,e], Ulman Lindenberger [a,d,*]

[a] Center for Lifespan Psychology, Max Planck Institute for Human Development, Berlin, Germany
[b] Lise Meitner Group for Environmental Neuroscience, Max Planck Institute for Human Development, Berlin, Germany
[c] Department of Psychiatry and Psychotherapy, University Medical Center Hamburg-Eppendorf, Germany
[d] Max Planck UCL Centre for Computational Psychiatry and Ageing Research, London, UK, & Berlin, Germany
[e] Department of Psychology, MSB Medical School Berlin, Berlin, Germany

ARTICLE INFO

Keywords:
Multi-trait multi-method (MTMM) model
Grey matter
Cognition
Healthy aging
Structural equation modelling

ABSTRACT

According to the maintenance hypothesis (Nyberg et al., 2012), structural integrity of the brain's grey matter helps to preserve cognitive functioning into old age. A corollary of this hypothesis that can be tested in cross-sectional data is that grey-matter structural integrity and general cognitive ability are positively associated in old age. Building on Köhncke et al. (2021), who found that region-specific latent factors of grey-matter integrity are positively associated with episodic memory ability among older adults, we examine associations between general factors of grey-matter integrity and a general factor of cognitive ability in a cross-sectional sample of 1466 participants aged 60–88 years, 319 of whom contributed imaging data. Indicator variables based on T1-weighted images (voxel-based morphometry, VBM), magnetization-transfer imaging (MT), and diffusion tensor imaging-derived mean diffusivity (MD) had sufficient portions of variance in common to establish latent factors of grey-matter structure for a comprehensive set of regions of interest (ROI). Individual differences in grey-matter factors were positively correlated across neocortical and limbic areas, allowing for the definition of second-order, general factors for neocortical and limbic ROI, respectively. Both general grey-matter factors were positively correlated with general cognitive ability. For the basal ganglia, the three modality-specific indicators showed heterogenous loading patterns, and no reliable associations of the general grey-matter factor to general cognitive ability were found. To provide more direct tests of the maintenance hypothesis, we recommend applying the present structural modeling approach to longitudinal data, thereby enhancing the physiological validity of latent constructs of brain structure.

Introduction

Many cognitive abilities decline in later adulthood [40] with large individual differences in the rate of decline [8,46]. According to the maintenance hypothesis [27–29], older individuals' overall levels of cognitive performance are assumed to reflect the degree to which their brains maintain youth-like anatomical macro- and microstructure as well as neurochemical, vascular, and metabolic

* Corresponding author.
E-mail address: lindenberger@mpib-berlin.mpg.de (U. Lindenberger).

https://doi.org/10.1016/j.nbas.2023.100103
Received 15 June 2023; Received in revised form 21 November 2023; Accepted 22 November 2023
Available online 7 December 2023
2589-9589/© 2023 The Author(s). Published by Elsevier Inc. This is an open access article under the CC BY-NC-ND license (http://creativecommons.org/licenses/by-nc-nd/4.0/).

functions [4,23,26,28,50].

Neuroimaging techniques such as T1-weighted structural imaging and diffusion tensor imaging (DTI) approximate macrostructural properties of brain tissues at various levels of granularity. Despite recent advances [51,52], the mapping of these properties onto physiologically interpretable constructs remains a challenge. Recently, attempts have been made to triangulate the degree of grey-matter structural integrity by combining different imaging modalities into a latent construct [20,21]. From a covariance modelling perspective, structural integrity is conceived as the variance that is shared across different imaging modalities, in the sense that individuals with more preserved structural integrity would tend to score higher across various indicators of structural properties. In earlier work, we have established such multi-modal indices of structural integrity in amygdala [21], and in a number of ROIs belonging to the episodic-memory network [20]. Here, we extend this multivariate-modelling approach to grey-matter ROIs across most regions of the brain, including neocortex, the limbic system, and the basal ganglia, with the intent to obtain a broader picture of individual differences in grey-matter structural integrity. Second, we extend our representation of cognitive ability beyond episodic memory to working memory and reasoning. This allows us to establish a general factor of cognitive ability across domains, and to examine the relationship between general factors of grey-matter integrity and a general factor of cognitive ability in old age.

In contrast to longitudinal work [13,14,19,32], the present analyses are cross-sectional in nature and do not provide a direct test of the maintenance hypothesis. With these analyses, we tested the more modest proposition that grey-matter integrity and cognitive ability are positively associated in old age. This proposition is based on the assumption that associations between constructs representing grey matter and constructs representing cognition age express the combined outcome of individual differences in normal aging and more stable individual differences that have emerged during earlier stages of ontogeny [16,34,48]. Hence, we expect a positive association between grey-matter integrity and cognition in old age.

In line with Köhncke et al. [20], we derived grey-matter probability from voxel-based morphometry (VBM; [2], which is based on signal intensity on T1-weighted structural MR scans. VBM is commonly used as an indicator of grey-matter volume. As indicators of microstructure, we used the magnetization-transfer (MT) ratio derived from MT imaging, and mean diffusivity (MD) derived from diffusion tensor imaging (DTI). MT imaging [42,43] is based on the transfer of energy and related magnetization exchange between mobile water protons and protons that are immobilized by macromolecules as part of brain tissue [53]. MT ratio values depend on the content and concentration of macromolecules bound to water molecules in relation to free water molecules. Lower MT ratio values can result from an increase in the mobile proton pool, occurring as a result of inflammation and oedema, or a decrease in the semi-solid proton pool, associated with cell damage, axonal loss, and demyelination [43].

DTI measures patterns of water diffusion. MD is a DTI-derived metric that reflects the rate of water diffusion in all directions within an imaged voxel [31]. It is commonly regarded as an index of white-matter microstructural integrity, but also can be informative of grey-matter microstructural properties and age-related differences therein [1,15], with lower MD corresponding to a denser structure, presumably indicating more cell membranes and intracortical myelin [15,45].

We hypothesized that, within a given ROI, these three macro- and microstructural indicators –VBM, MT, and MD– would share variance, thereby giving rise to ROI-based latent factors of tissue structural integrity. Based on our previous findings, we expected one such factor of integrity to emerge for each ROI. We also expected that ROIs within larger areas of the brain (neocortex, limbic system, and basal ganglia) might share variance so that second-order factors of grey-matter integrity across ROIs can be established for each of the three systems. As many brain regions work together to enable cognitive functioning, it is reasonable to expect that these second-order, or general, factors of grey-matter integrity (GGM), should it be possible to establish them in the first place, would be positively associated with general cognitive ability (GCA).

Methods

Participants and study design

For the present analyses, we used data from healthy older participants of the Berlin Aging Study II (BASE-II), a multi-institutional and multidisciplinary study assessing variables from a wide range of domains [3]. Participants completed a comprehensive cognitive examination at several waves, of which we use the first wave data here [9]. Before or after the cognitive assessment, a subsample of eligible participants was invited to take part in a separate MRI session (median time interval 8 weeks, IQR = 19 weeks, range = –27 to 111 weeks). Eligibility criteria included: (a) no medication that is known to potentially affect memory function; (b) no history of head injuries; (c) no medical (e.g., heart attack), neurological (e.g., epilepsy), or psychiatric disorders (e.g., depression); and (d) a completion of at least 8 years of education. BASE-II includes a larger sample of persons above age 60 years and a smaller sample of participants in early adulthood. Here, we selected only data from participants above age 60, of whom 1,466 had completed cognitive testing; of these 1,466 individuals, 319 had also taken part in MR imaging. We had to exclude nine cases with compromised cognitive data, two of whom also formed part of the MR subsample. We then excluded univariate outliers on a variable-by-variable basis, and multivariate outliers with highly unlikely combinations of values, $p < .0001$, of robust Mahalanobis distances, which were detected using the R-package faoutlier, version 0.7.2 [6], method "mve." We identified multivariate outliers separately for the cognitive data in the total sample (n = 1,477, 11 outliers found, resulting in the effective sample of 1,466 individuals) and for the grey-matter variables in the MR sample per group of ROIs, with 10 multivariate outliers in the neocortical ROIs, 4 in the limbic ROIs, and 8 in basal ganglia ROIs. For further information on the sample, see the Supplementary Materials. The Ethics Committee of the Max Planck Institute for Human Development approved the behavioral testing part of the study, and the Ethics Committee of the German Psychological Society (Deutsche Gesellschaft für Psychologie, DPGs) approved the imaging part. Participants received monetary compensation for their participation in the cognitive and imaging sessions and provided informed consent in accordance to the Declaration of Helsinki.

MRI acquisition

Images were acquired on a Siemens Tim Trio 3 T scanner (Erlangen, Germany) using a 32-channel head coil. The T1 images were obtained using a three-dimensional T1-weighted magnetization prepared gradient-echo (MPRAGE) sequence based on the ADNI protocol (https://www.adni-info.org; repetition time (TR) = 2500 ms; echo time (TE) = 4.77 ms; TI = 1100 ms, acquisition matrix = 256 × 256 × 176, flip angle = 7; 1 x 1 x 1 mm^3 voxel size). Diffusion-weighted images were obtained with a single-shot diffusion-weighted spin-echo-refocused echo-planar imaging sequence (FOV 218 mm × 218 mm; 128 × 128 matrix interpolated to 256 × 256; TE = 98 ms; TR = 11,000 ms; 73 slices; slice thickness 1.7 mm; b-value 1000 s/mm^2; 60 directions). MT ratio images consisting of two volumes were acquired with identical settings (transversal, 256 × 256 pixels, TE = 5.5 ms, TR = 28 ms, 48 slices, voxel size 1 mm × 1 mm × 3 mm). The first sequence (MT) was acquired with a magnetic saturation pulse (1200 Hz off-resonance, 16 ms) and the second (noMT) without a magnetic saturation pulse, resulting in a proton-density-like image.

MR preprocessing

Voxel-based morphometry (VBM). Structural data were processed with CAT12 (Computational Anatomy Toolbox 12, Structural Brain Mapping group, Jena University Hospital, Jena, Germany), a toolbox that is implemented in SPM12 (Statistical Parametric Mapping, Institute of Neurology, University College London, UK) for voxel-based morphometry analysis of imaging data. We applied the CAT12 default cross-sectional pre-processing stream, which implements correction of the T1-weighted images for bias-field inhomogeneities, segmentation into grey matter, white matter, and CSF, and spatially normalized using the DARTEL (Diffeomorphic Anatomical Registration Through Exponentiated Lie Algebra) algorithm. Modulation with Jacobian determinants was applied in order to preserve the volume of a particular tissue within a voxel leading to a measure of volume of grey matter. Grey-matter images were used for the current set of analyses and smoothed with a Gaussian kernel of 8 mm (full width at half maximum).

Magnetization transfer imaging (MTI). The MT maps for each participant were calculated on a voxel-by-voxel basis according to the formula MT ratio = (noMT − MT) / noMT. The data were then normalized into MNI space.

Diffusion tensor imaging (DTI). Diffusion-weighted images were pre-processed using the FSL software package [18,44], version 5.0. This included corrections of potential head movement and inspection of image quality. The first non-diffusion weighted image of each individual image set was used as a brain mask. The difference in alignment between this initial image and recurrent ones in the sequence was estimated using FLIRT (FMRIB's Linear Image Registration Tool; [18]) and then corrected for by means of re-alignment. The resulting data was then processed via FSL's *dtifit* to fit a diffusion tensor model at each voxel and obtain the MD values. The MNI-based maps were produced using the standard TBSS pipeline [44].

ROI extraction and adjustment for differences in intracranial volume

Mean values of CAT12/VBM, MD and MT ratio were extracted bilaterally from ROIs defined by the Automated Anatomical Labelling (AAL) atlas [47]. ROI masks were fitted in MNI space after normalization to a standard template.

We used intracranial volume (ICV from CAT12) to adjust the VBM values for each ROI via the analysis of covariance formula [35]: adjusted volume = raw volume − b * (ICV − mean ICV), where b is the slope of regression of the appropriate ROI volume on ICV.

Cognitive assessment

All BASE-II participants were invited to two cognitive test sessions with an exact interval of seven days and at the same time of day to avoid circadian confounding effects on performance. Each session lasted about 3.5 h. Participants were tested in groups of 4–6 individuals. Each group was instructed via a standardized session manual. Each task started with a practice trial to ensure that every participant understood the task. Depending on the task, responses were given via button boxes, the computer mouse, or a keyboard.

The cognitive battery of BASE-II covers key cognitive abilities measured by 21 tasks, 4 of which assess aspects of episodic memory, 3 of which assessed working memory, and 3 reasoning. The tasks are described in more detail elsewhere [9,20].

Episodic memory tasks. (i) The *Verbal Learning and Memory Task* assessed free recall of 15 auditorily presented words that were repeatedly presented in the same order in five learning trials. Participants typed the words they recalled on the keyboard. We used the sum of remembered words across all learning trials as the score indicating performance in this task. (ii) *Face–Profession,* testing associative recognition memory 5 min after incidental encoding of 45 images of faces combined with a written profession title. Participants were instructed to judge for each face–profession pair whether they matched well. During recall, participants were presented with 27 old, 9 new, and 18 rearranged (newly combined) pairs and asked to provide old-new judgements. A participant's performance score was computed as hits (correctly identified as previously seen pairs) minus false alarms to rearranged pairs. (iii) The *Scene Encoding* task assessed recognition memory of 88 incidentally encoded scenes. Participants were presented with images of scenes and were given the task to judge whether the scenes were indoors or outdoors (with 44 of each type). Recognition was tested after a delay of 2.5 h. Participants were shown 44 old and 44 new scenes in random order (22 indoors and 22 outdoors in each of the old and the new set). Performance scores were computed as hits minus false alarms. (iv) *Object Location* task to assess recall of deliberately encoded object locations. Sequences of 12 photographs of real-world objects were displayed at different locations in a 6-by-6 locations grid. After the sequence, objects appeared at the side of the screen and participants were asked to move pictures to the location they were first presented at, by means of clicking the picture and the location with the mouse. The task consisted of one practice trial and two test trials. The sum of correct placements across the two test trials is used in this study.

Working memory tasks. (i) *Spatial Updating Task.* Participants were presented with two (load 2 condition) or three (load 3 condition) 3-by-3 grids for 4 s each. In each of these grids, a blue dot was presented in one of the nine locations. Those two/three locations had to be memorized and updated according to shifting operations that are indicated by arrows appearing below the corresponding field. After four/six updating operations, the two/three grids reappear and the participants indicate the updated positions by mouse click. After 10 practice blocks, of which 8 were with load 2-condition and 2 with load-3 condition, 8 blocks of each condition were conducted. A sum score of hits across all 16 blocks is used here. (ii) *Letter Updating Task*. Participants were presented with 7, 9, 11, or 13 letters (A, B, C, or D) in a sequence. After a sequence, they were requested to report the last three letters by pressing buttons corresponding to the four letters in the correct order. The scores are the sum of recalled letters across 16 sequences. (iii) *Numerical N-back Task*. Three one-digit numbers (ranging from 0 to 9) were presented sequentially in three cells situated horizontally followed by the next sequence of three digits (presentation time = 1500 ms/inter-stimulus-interval = 500 ms). This cycle was repeated 30 times. In each cycle, participants indicated by button press whether the current stimulus matched the stimulus shown three steps earlier. The score we extracted comprises mean hit rate across 6 trials with 30 runs each.

Reasoning tasks. (i) *Figural Analogies.* This task follows the format "A is to B as C is to?". A pair of abstract figures with a logical link was presented, and a single figure was presented next to it, with 5 possible figures to choose from. Participants were instructed to choose a figure that would match with the single figure following the same rule as the example pair. The task terminated when subjects made three consecutive errors, when they reached the maximum time limit (10 min), or after they had reached the last test item. Items were ordered by difficulty. Scores were the sums of correct responses to maximally 22 items. *(ii) Practical Problems.* Everyday problems related to, e.g., the times in a bus schedule, instructions for medication, or ingredients for a recipe were presented, with four alternative responses to choose from by mouse click. The task terminated when subjects made three consecutive errors, when they reached the maximum time limit (10 min), or after they had reached the last test item. Items were ordered by difficulty. Scores were the sums of correct responses to maximally 18 items. *(iii) Letter Series.* Each item contained five letters followed by a question mark (e.g., c e g i k?), five response alternatives were to be chosen from and indicated with a mouse click. The letter series followed simple rules such as +1, –1, +2, or +2 +1 with respect to the letters' positions in the alphabet. The task terminated when subjects made three consecutive errors, when they reached the maximum time limit (10 min), or after they had reached the last test item. Items were ordered by difficulty. Scores were the sums of correct responses to maximally 22 items.

Statistical analyses

For two reasons, we used structural equation modelling (SEM) to investigate the relationships between cognitive performance and grey-matter integrity. First, for each ROI, SEM allows a latent factor of structural integrity that captures the variance shared across the three brain-imaging modalities to be estimated. By separating the shared variance (i.e., what is common across measures) from unique, modality-specific variance (i.e., what is specific to each measurement), we acquired a more reliable and potentially more valid estimate of brain integrity. We also defined latent method factors for each modality, VBM, MT, and MD, that capture the variance common to a given modality across all. As a consequence, the estimates of residual variance in our model represent variance that is neither shared by all ROIs in a given modality nor shared by all modalities in a given ROI and is therefore not of interest (e.g., can be considered as measurement error).

Second, we used SEM to link general structural integrity with GCA. In this context, a particular virtue of SEM is that we can model grey-matter integrity for each of the ROIs (e.g., prefrontal cortex, parietal cortex, occipital cortex) and also estimate a general grey-matter integrity factor across all ROIs within a given larger area (neocortex, limbic areas, basal ganglia). Similarly, we can model the cognitive domains (working memory, episodic memory, reasoning) as well as a GCA factor across domains. Joining both hierarchical factor models, we can estimate how GCA is related to general grey-matter integrity and then investigate whether there are additional associations between the three specific cognitive abilities and ROIs over and above the association observed at the general level. We can also integrate relevant covariates such as chronological age, gender, and education into the model to investigate the extent to which the associations between brain integrity and cognition are confounded with these variables.

We specified and estimated structural equation models in lavaan [37], version 0.6–12, a SEM package in R [36], version 4.2.3 (2023–03-15). To account for missing data, we used full information maximum likelihood estimation. Given that large differences in measurement scales, as present in our data, typically pose problems for numerical optimization algorithms, all observed variables were rescaled. We chose a scale with a mean of 5 and a standard deviation of 2. To evaluate the fit of the final models, we used the Root Mean Square Error of Approximation (RMSEA), the Comparative Fit Index (CFI), and the Standardized Root Mean Residual (SRMR). We interpret CFI > 0.90, RMSEA < 0.08, and SRMR < 0.8 as indications of acceptable model fit [41]. To assess statistical significance of individual parameter estimates within a model, we used the likelihood ratio test. That is, we compared the model with the parameter of interest freely estimated, to a nested model with this parameter fixed to zero, and compared whether the χ^2 difference between the models indicated a significant difference in fit at a 5 % significance level. For loadings and variance parameters, we used the Z-value (or

Wald statistic; parameter estimate divided by its standard error) from the lavaan output as the significance test.

In a first step, we specified separate confirmatory factor analyses to validate each latent-integrity factor model for the selected ROIs defined by the indicators representing the three imaging modalities. In a next set of analyses, we combined the individual, fully saturated models to one of three larger structural equation models, in which we combined the ROIs according to larger anatomical areas into three different models: (A) the neocortical model with the ROIs dorsolateral prefrontal cortex (DL), medio-orbitofrontal cortex (MO), precuneus (PRE), parietal cortex (PAR), occipital cortex (OCC), and Heschl's gyrus (HES); (B) the limbic model with the ROIs dorsolateral parahippocampal cortex (PHG), hippocampus (HC), anterior cingulate cortex (ACC), amygdala (AMY); and (C) the basal ganglia model with the ROIs caudate (CAU), putamen (PUT), nucleus accumbens (NAC), and pallidum (PAL).[1] First, we established a model with one latent factor for each ROI within that area and three method factors (VBM, MT, MD). The ROI factors were allowed to covary, and the methods factors were also allowed to covary. This type of model is known as a MTMM (multi-trait multi-method) model [5,11]. It is the appropriate measurement model if multiple characteristics (usually traits, but here, ROIs) are each measured by several distinct measures (usually raters, but here, imaging modalities), yielding a latent integrity factor for each ROI and a latent method factor for each imaging modality. The latent scales of both the ROI factors and method factors were identified by fixing the loading of a reference indicator to one (Fig. 1). In a next step, we added a second-order factor of general grey-matter integrity (GGM) with freely estimated loadings on all ROIs and a variance fixed to 1 to define the scale of the factor. To establish domain-specific ability factors, we combined the tasks for each domain in a factor model, as in previous work [9,21]. We then defined a factor of GCA, or g, as a second-order factor expressing the shared variance of the three domain-specific ability factors. The domain factors were scaled by the first loading, the GCA factor by a variance of 1.

In subsequent analyses, we added age and sex as observed covariates to statistically control for age and sex differences in GCA and general grey-matter integrity. In addition, we also tested whether education was related to either of these general factors.

Models that entailed only brain data were fitted to data from the MR sample, and models that entailed episodic memory data were fitted to data from the total sample, under the assumption that the MR data were missing at random [38,39]. This assumption holds as long as missingness in the grey-matter variables is either completely random or can be explained by variables in the model.

Results

Latent factors were estimable for all ROIs, but with substantial differences in loading homogeneity. The indicators from dorsolateral PFC and medio-orbitofrontal cortex were so highly correlated that we decided to merge them into a single PFC ROI, as in [20]. The fit of the neocortical brain-only model was within the acceptable range ($CFI = 0.90$, $RMSEA = 0.08$, $SRMR = 0.08$). The fits of the limbic and basal ganglia brain-only models were slightly lower than acceptable (limbic: $CFI = 0.89$, $RMSEA = 0.10$. $SRMR = 0.10$; basal ganglia: $CFI = 0.88$, $RMSEA = 0.12$, $SRMR = 0.11$).

Given that the main rationale of our analyses was to build models that include both brain and cognition, we decided to continue working with these models despite their inferior fit, and examined them more closely. Loading patterns across the three modalities were more homogenous in neocortical areas than in limbic areas, and most heterogeneous in basal ganglia (Table 1A–C: loadings), with putamen and pallidum even switching signs for some of the loadings. Across most ROIs, the VBM measures showed the weakest loadings, indicating that the variance of the latent ROI integrity factor contained a greater share of the microstructural indicators MT and MD. The MD indicators' loadings were negative (except for putamen), in line with the interpretation that higher MD values indicate a less dense structure such that MD is negatively associated with MT. ROIs in the basal ganglia tended to diverge from the loading pattern in neocortical and limbic ROIs; specifically, in caudate, the estimates for MD and MT loadings were an order of magnitude larger than the volumetric indicator's loading (the reference loading for scaling) and came with large standard errors. In putamen and pallidum, MD loadings and MT loadings partly switched sign.

For a graphical representation of the models and the most important parameter estimates, see Fig. 1. For a full list of parameter estimates, see Table S3 A–C (full sample) and D–F (MR subsample, brain-only model) in the Supplementary Materials.

The second-order factors captured common variance across ROIs in all three groups of ROIs. See Table 2A–C for the loadings on GGM factor.

Method factors captured modality-specific variance in all three models. We estimated covariances among methods factors in the models without covariates first. In the neocortical and limbic model, all method factors were correlated with one another, with weaker correlations between VBM and MT (NEOCORTEX: $r_{V,MT} = 0.23$, $p = .02$; $r_{V,MD} = -0.451$, $p < 0.001$; $r_{MT,MD} = -0.73$, $p < .001$; LIMBIC: $r_{V,MT} = 0.22$, $p = .079$; $r_{V,MD} = -0.52$, $p < .001$; $r_{MT,MD} = -0.64$, $p < .001$; BASAL GANGLIA: $r_{V,MT} = -0.22$, $p = .06$; $r_{V,MD} = 0.35$, $p = .001$; $r_{MT,MD} = -0.57$, $p < .001$). Non-significant (Wald test) correlations among method factors were tested with a likelihood ratio test to find out whether they can be constrained to zero without significant loss of model fit. None of the methods factor covariances could, so we had to assume that they are non-orthogonal.

In the next step, we added the factor models for episodic memory, working memory, and reasoning, and GCA factor to the model,

[1] Originally, our aim was to fit an overall hierarchical brain model to the data that would encompass all ROIs investigated in the present study. This model did not converge, presumably due to the fact that the number of parameters was too high relative to the number of participants. By grouping the regions based on broad anatomical characteristics into three submodels, we were able to keep the size of the models within bounds that allowed for model convergence. We also fitted ROI-specific measurement models as a preparatory step to find out whether loading patterns looked similar across ROIs. We noticed that subcortical structures deviated from the loading patterns observed in the other ROIs, which was a further reason to group ROIs according to broad anatomical categories, and refrain from trying to establish an overall model.

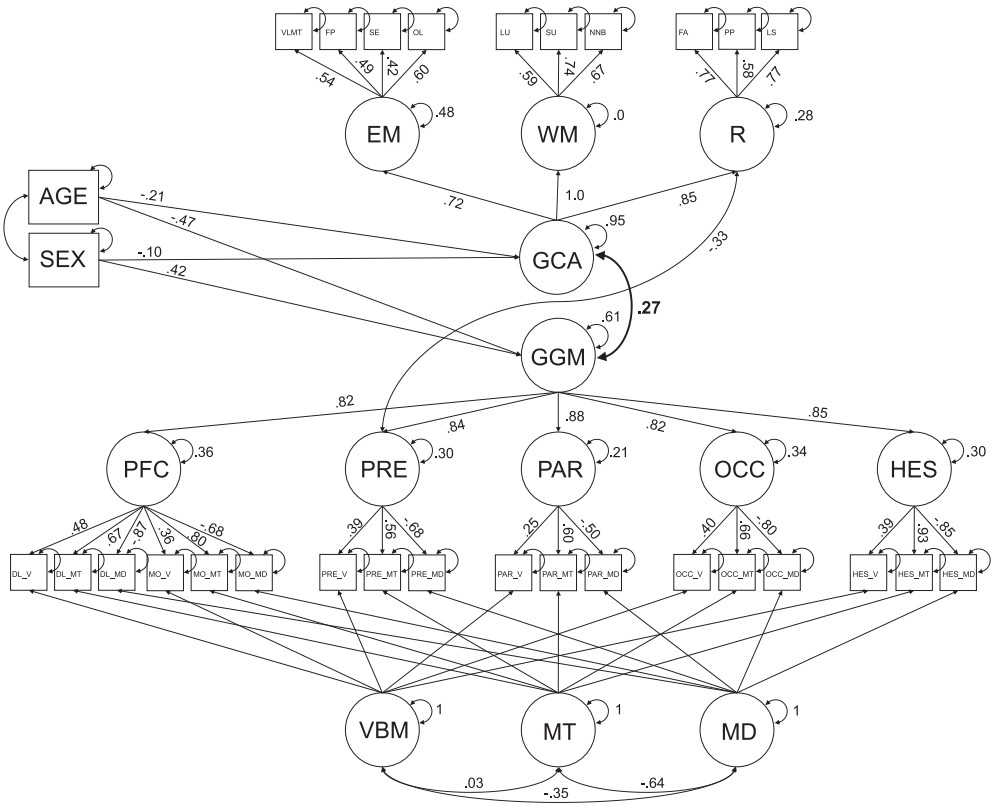

Fig. 1A. Multi-trait multi-method (MTMM) model of brain structure: Submodel for neocortical ROIs (see Fig. 1B for abbreviations).

applied it to the data set with a larger sample size with cognitive data (n = 1,466) and estimated the correlations between GGM and GCA, for each of the three integrity models separately. First, we allowed for residual covariances of all cognitive domain factors with all ROI factors, and then, we constrained the non-significant residual covariances to zero to simplify the models. The fit indices of the final neocortical and limbic models were all within the acceptable range (neocortical: *CFI* = 0.94, *RMSEA* = 0.03, *SRMR* = 0.06; limbic: *CFI* = 0.92, *RMSEA* = 0.03, *SRMR* = 0.08). For the basal ganglia model, CFI and RMSEA were within the acceptable range, but the SRMR slightly exceeded the acceptable value of 0.08 (*CFI* = 0.94, *RMSEA* = 0.03, *SRMR* = 0.09).

GCA was associated with neocortical GGM ($r_{GCA,GGM} = 0.29$, $\chi^2\Delta_{(df=1)} = 18.01$, $p < .001$) and limbic GGM ($r_{GCA,GGM} = 0.28$, $\chi^2\Delta_{(df=1)} = 18.28$, $p < .001$), but not with basal ganglia GGM ($r_{GCA,GGM} = 0.10$, $\chi^2\Delta_{(df=1)} = 2.02$, $p = .15$). When we added age and sex as predictors, the associations of neocortical and limbic GGM with GCA were somewhat attenuated but still significantly different from zero (NEOCORTEX: $r_{GCA,GGM} = 0.27$, $\chi^2\Delta_{(df=1)} = 11.72$, $p < .001$; LIMBIC: $r_{GCA,GGM} = 0.25$, $\chi^2\Delta_{(df=1)} = 14.41$, $p < .001$).

In the case of the basal-ganglia model, we did not add covariates, as there was no significant GGM-GCA association in the first place. Note also that the loading pattern was quite different for the basal-ganglia model, such that the loadings for caudate MD and MT were about ten times as high as the VBM loading. Also, putamen and pallidum showed negative MT loadings, and putamen a positive MD loading (see Table 1C). All in all, the loadings pattern observed for the basal ganglia was counter to expectations, raising doubts about the content validity of the resulting latent factors.

In the neocortical model, the reasoning factor had a negative residual covariance with precuneus. Apparently, this factor was less strongly associated with reasoning than captured by the general GCA-GGM association.

Tested in brain-only models, education was neither related to neocortical GGM ($\beta_{std} = 0.07$, $p = .29$) nor to limbic GGM ($\beta_{std} = 0.06$, $p = .35$). Therefore, we refrained from including education as a covariate.

Discussion

We recently suggested combining multi-modal imaging with confirmatory factor analysis to approximate constructs of brain structural integrity [20,21]. Here, we extended this approach to a comprehensive set of brain regions and a larger set of cognitive abilities. Informed by the maintenance hypothesis of cognitive aging [23,28], we expected a positive association between general factors of grey-matter integrity and cognitive ability in old age.

Similar to earlier findings focused on episodic memory by Köhncke et al. [20], we found that three different measures of brain-tissue structural characteristics, VBM, MT and MD, shared substantial variance in many ROIs of the human brain. Across the

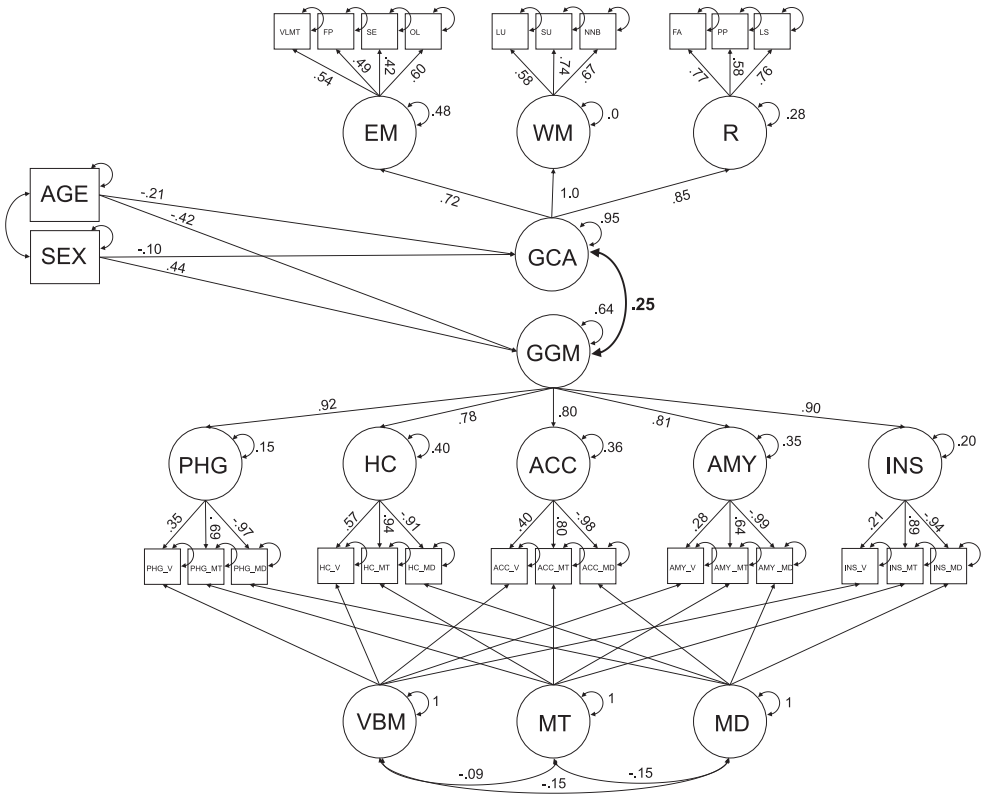

Fig. 1B. Multi-trait multi-method (MTMM) model of brain structure: Submodel for limbic ROIs.
Note. Rectangles represent observed variables, circles latent variables. Single-headed arrows represent regression parameters and loadings, double-headed arrows variances (where both arrows point to the same variable) and covariances (where they connect two variables). Parameter estimates are standardized. Residual variances of the observed variables, variances and covariances of the covariates, and loadings of the methods factors were freely estimated but estimates are not shown here for sake of clarity. EM = episodic memory; VLMT = Verbal Learning and Memory Task; FP = Face–Profession task; SE = Scene Encoding task; OL = Object Location task; WM = Working Memory; LU = Letter Updating; SU = Spatial Updating; NNB = Number N-back; R = Reasoning; FA = Figural Analogies; PR = Practical Problems; LS = Letter Series; PFC = prefrontal cortex; PRE = precuneus; PAR = parietal cortex; OCC = occipital cortex; HES = Heschl's gyrus; PHG = parahippocampal gyrus; HC = hippocampus; ACC = anterior cingulate cortex; AMY = amygdala; INS = insula; _V = voxel-based morphometry; _MT = magnetization transfer imaging; _MD = mean diffusivity.

neocortex and large parts of the limbic system, the two microstructural parameters, MT and MD, had larger loadings on the ROI-wise integrity factors than the index of grey-matter probability, VBM. Thus, the microstructural properties assessed by MT and MD were more closely related to each other than each of them was to an estimate of grey-matter volume.

Building upon the ROI-specific grey-matter factors, we established general grey-matter factors. We found that the neocortical and the limbic general grey-matter factors were positively associated with general cognitive ability. Thus, extending the earlier analysis of Köhncke et al. [20], we show that the link between grey-matter integrity and cognition in old age generalizes across a comprehensive set of neocortical and limbic ROIs on the brain side, and to general cognitive ability, on the behavioral side. These findings are in good agreement with the notion that brain maintenance has a general component, in addition to components that are more specific to select regions of the brain and select cognitive functions [19]. It has to be kept in mind, however, that the general grey-matter factors established in the present study accounted for only six to seven percent of the variance in general cognitive ability. Clearly, the bulk of the brain-cognition link remains to be uncovered.

In contrast to neocortical and limbic areas, findings for the basal ganglia were less clear. The factor loading patterns for the caudate, putamen, and pallidum deviated from the expected pattern that was observed in most other regions, thereby reducing the interpretability of the basal ganglia model. In the cases of the putamen and the pallidum, the sign of the MT factor loadings switched from positive to negative while the sign of the VBM loadings remained positive; hence, the relationship between the indictors was opposite to that observed in other regions. We had assumed that lower MT ratio values would result from an increase in the mobile proton pool as a result of inflammation and oedema, or a decrease in the semi-solid proton pool as a result of cell damage, axonal loss and demyelination. In retrospect, however, it seems plausible that in the basal ganglia of older adults, and especially in the putamen and the pallidum [12], MT values might predominantly signal the presence of iron deposits, such that higher values reflect greater iron accumulation instead of more intact tissue. This post-hoc interpretation would be consistent with the altered factor loading pattern observed here. In addition, the microstructure of subcortical nuclei differs from the laminar structure of cortical areas, which may also

Table 1A
NEOCORTEX ROI factor loadings.

ROI Factor	Indicator variable	Loading parameter estimate	Standard error	z-value	p-value	Standardized parameter estimate
PFC	DL_V	1.000	0.000			0.489
PFC	DL_MT	1.453	0.224	6.488	0.000	0.678
PFC	DL_MD	−1.878	0.253	−7.429	0.000	−0.870
PFC	MO_V	0.731	0.141	5.172	0.000	0.358
PFC	MO_MT	1.675	0.247	6.792	0.000	0.803
PFC	MO_MD	−1.481	0.207	−7.170	0.000	−0.688
PRE	PRE_V	1.000	0.000			0.399
PRE	PRE_MT	1.495	0.298	5.017	0.000	0.579
PRE	PRE_MD	−1.751	0.324	−5.409	0.000	−0.680
PAR	PAR_V	1.000	0.000			0.252
PAR	PAR_MT	2.533	0.801	3.162	0.002	0.624
PAR	PAR_MD	−2.096	0.645	−3.248	0.001	−0.516
OCC	OCC_V	1.000	0.000			0.412
OCC	OCC_MT	1.682	0.281	5.978	0.000	0.671
OCC	OCC_MD	−2.026	0.295	−6.867	0.000	−0.803
HES	HES_V	1.000	0.000			0.392
HES	HES_MT	2.423	0.426	5.690	0.000	0.935
HES	HES_MD	−2.217	0.388	−5.711	0.000	−0.846

PFC = prefrontal cortex; PRE = precuneus; PAR = parietal cortex; OCC = occipital cortex; HES = Heschl's gyrus; _V = voxel-based morphometry; _MT = magnetization transfer imaging; _MD = mean diffusivity; estimates from brain-only model with covariates age and sex fit to data from MR subsample.

Table 1B
LIMBIC ROI factor loadings.

ROI Factor	Indicator variable	Loading parameter estimate	Standard error	z-value	p-value	Standardized parameter estimate
PHG	PHG_V	1.000	0.000			0.353
PHG	PHG_MT	2.139	0.384	5.571	0.000	0.691
PHG	PHG_MD	−2.980	0.515	−5.788	0.000	−0.974
HC	HC_V	1.000	0.000			0.566
HC	HC_MT	1.769	0.183	9.690	0.000	0.944
HC	HC_MD	−1.733	0.169	−10.242	0.000	−0.908
ACC	ACC_V	1.000	0.000			0.403
ACC	ACC_MT	2.037	0.357	5.710	0.000	0.798
ACC	ACC_MD	−2.553	0.428	−5.967	0.000	−0.984
AMY	AMY_V	1.000	0.000			0.280
AMY	AMY_MT	2.479	0.570	4.349	0.000	0.634
AMY	AMY_MD	−3.818	0.819	−4.664	0.000	−0.996
INS	INS_V	1.000	0.000			0.213
INS	INS_MT	4.439	1.518	2.925	0.003	0.885
INS	INS_MD	−4.657	1.571	−2.963	0.003	−0.943

PHG = parahippocampal gyrus; HC = hippocampus; ACC = anterior cingulate cortex; AMY = amygdala; INS = insula; _V = voxel-based morphometry; _MT = magnetization transfer imaging; _MD = mean diffusivity; estimates from brain-only model with covariates age and sex fit to data from MR subsample.

Table 1C
BASAL GANGLIA ROI factor loadings.

ROI Factor	Indicator variable	Loading parameter estimate	Standard error	z-value	p-value	Standardized parameter estimate
CAU	CAU_V	1.000	0.000			0.131
CAU	CAU_MT	6.217	3.498	1.777	0.076	0.861
CAU	CAU_MD	−5.256	2.933	−1.792	0.073	−0.675
PUT	PUT_V	1.000	0.000			0.488
PUT	PUT_MT	−0.831	0.204	−4.072	0.000	−0.399
PUT	PUT_MD	0.261	0.146	1.781	0.075	0.128
NAC	NAC_V	1.000	0.000			0.579
NAC	NAC_MT	0.959	0.150	6.385	0.000	0.569
NAC	NAC_MD	−1.150	0.156	−7.390	0.000	−0.685
PAL	PAL_V	1.000	0.000			0.437
PAL	PAL_MT	−0.951	0.303	−3.140	0.002	−0.402
PAL	PAL_MD	−0.355	0.364	−0.976	0.329	−0.153

CAU = caudate nucleus; PUT = putamen; NAC = nucleus accumbens; PAL = pallidum; _V = voxel-based morphometry; _MT = magnetization transfer imaging; _MD = mean diffusivity; estimates from brain-only model without covariates fit to data from MR subsample.

Table 2A
Neocortex ROI loadings on GGM.

G Factor	ROI	Loading parameter estimate	Standard error	z-value	p-value	Standardized parameter estimate
GGM	PFC	0.613	0.092	6.673	0.000	0.821
GGM	PRE	0.511	0.101	5.062	0.000	0.850
GGM	PAR	0.344	0.106	3.260	0.001	0.893
GGM	OCC	0.512	0.087	5.908	0.000	0.817
GGM	HES	0.507	0.097	5.229	0.000	0.843

Table 2B
Limbic ROI loadings on GGM.

G Factor	ROI	Loading parameter estimate	Standard error	z-value	p-value	Standardized parameter estimate
GGM	HC	0.663	0.084	7.858	0.000	0.776
GGM	PHG	0.486	0.087	5.560	0.000	0.923
GGM	ACC	0.504	0.090	5.616	0.000	0.801
GGM	AMY	0.343	0.078	4.417	0.000	0.809
GGM	INS	0.296	0.102	2.904	0.004	0.896

Table 2C
Basic ganglia ROI loadings on GGM.

G Factor	ROI	Loading parameter estimate	Standard error	z-value	p-value	Standardized parameter estimate
GGM	CAU	0.234	0.131	1.788	0.074	0.892
GGM	PUT	0.898	0.159	5.645	0.000	0.904
GGM	NAC	0.792	0.146	5.416	0.000	0.679
GGM	PAL	0.382	0.141	2.706	0.007	0.440

alter the relations between MT and MD, and their associations with VBM. For instance, atrophy in hippocampus is not closely related to atrophy in caudate [26], and it has been proposed that caudate volume might increase in compensation for hippocampal shrinkage [30].

Normal aging is marked by the loss of dendritic spines, dendritic arbors, synaptic density, and myelinated axons [17,25]; in addition, normal aging also involves loss of glia and small blood vessels [33]. All of these processes can contribute to differences in average tissue density as captured by MT and MD, and to differences in overall volume as captured by VBM. The relative contribution of these underlying biological properties is likely to differ between ROIs. In our previous paper linking cortical ROIs and the hippocampus to episodic memory [20], we suggested that cortical myelin might be the most prominent factor in terms of relative contributions to variations in the MR signal that affect all three parameters, MD, MT, and VBM. However, in the case of subcortical structures, the picture might be more complex, and the drivers of the associations might vary across them. It is worthwhile to follow up on these considerations using quantitative imaging techniques at higher resolution [10]. In addition, the links of human structural MR imaging to histology need to be strengthened [22,51].

By far the most serious limitation of the present findings is their cross-sectional nature. The present findings are consistent with a maintenance account of cognitive aging, but they do not provide a direct test of it. In particular, an unknown but possibly large portion of the positive association between grey-matter integrity and cognition might already have been present early in life, which would imply that contributions of differential maintenance to the magnitude of this association in old age are minor; for a general discussion of this issue, see [49].

It has been proposed that brain maintenance, defined as individual differences in preservation of brain integrity, can occur at the level of specific brain circuits and cognitive functions or at a more general level [27]. The longitudinal evidence on this matter is mixed. In line with general maintenance, Cox and colleagues reported that a broad, cortex-wide dimension of atrophy was associated with declines in general cognitive ability as well as visuospatial ability, processing speed, and memory [7]. In line with a general-as well as specific-maintenance account, Johansson and colleagues recently found a reliable association between MTL/hippocampal change and episodic memory change after accounting for the covariance among general factors of change in brain and cognition [19]. At first sight, the present cross-sectional findings may seem more consistent with the general maintenance account. However, given that the dimensionality of change cannot be inferred from cross-sectional data [24], this conclusion is not warranted. Rather, further longitudinal data with fine-grained information on physiological brain changes and behavioral changes are needed to examine this issue.

Conclusion

By extending our previous MTMM modelling work on data from BASE-II participants, we established general factors of grey-matter structural integrity across cortical and limbic regions, and found that both of these general factors are positively related to general

cognitive ability. Future research needs to extend the present approach to longitudinal observations, and to further clarify and improve the physiological validity of latent constructs of brain structure.

Funding

This work was supported by the European Commission as part of the Lifebrain Consortium (grant number 732592) within the Horizon 2020 programme. This project is also part of the EnergI consortium (grant number 01GQ1421B) funded by the German Federal Ministry of Education and Research. MCS was supported by the MINERVA program of the Max Planck Society.

Authorship Contributions

Ylva Köhncke: Conceptualization, data analysis, methodology, writing original draft; Simone Kühn: Conceptualization, methodology, supervision of data collection, processing of neuroimaging data, editing; Sandra Düzel: Conceptualization, supervision of data collection, editing; Myriam C. Sander: Conceptualization, editing; Andreas M. Brandmaier: Conceptualization, methodology, editing; Ulman Lindenberger: Conceptualization, methodology, revising original draft.

Declaration of competing interest

The authors declare that they have no known competing financial interests or personal relationships that could have appeared to influence the work reported in this paper.

Acknowledgements

We are grateful to the MRI team at the Max Planck Institute for Human Development, namely Sonali Beckmann, Nils Bodammer, Thomas Feg, Sebastian Schröder, and Nadine Taube, for their assistance, to the team leading the cognitive tests, and to all BASE-II participants. We also thank Julia Delius for editing an earlier version of this manuscript.

Appendix A. Supplementary data

Supplementary data to this article can be found online at https://doi.org/10.1016/j.nbas.2023.100103.

References

[1] Abe O, Yamasue H, Aoki S, Suga M, Yamada H, Kasai K, et al. Aging in the CNS: Comparison of gray/white matter volume and diffusion tensor data. Neurobiol Aging 2008;29(1):102–16. https://doi.org/10.1016/j.neurobiolaging.2006.09.003.
[2] Ashburner J, Friston KJ. Voxel-based morphometry: The methods. Neuroimage 2000;11:805–21. https://doi.org/10.1006/nimg.2000.0582.
[3] Bertram L, Bockenhoff A, Demuth I, Duzel S, Eckardt R, Li SC, et al. Cohort profile: The Berlin Aging Study II (BASE-II). Int J Epidemiol 2014;43(3):703–12. https://doi.org/10.1093/ije/dyt018.
[4] Cabeza R, Albert M, Belleville S, Craik FIM, Duarte A, Grady CL, et al. Maintenance, reserve and compensation: The cognitive neuroscience of healthy ageing. Nat Rev Neurosci 2018;19(11):701–10. https://doi.org/10.1038/s41583-018-0068-2.
[5] Campbell DT, Fiske DW. Convergent and discriminant validation by the multitrait-multimethod matrix. Psychol Bull 1959;56(2):81–105. https://doi.org/10.1037/h0046016.
[6] Chalmers RP, Flora DB. faoutlier: An R package for detecting influential cases in exploratory and confirmatory factor analysis. Appl Psychol Meas 2015;39(7):573–4. https://doi.org/10.1177/0146621615597894.
[7] Cox SR, Harris MA, Ritchie SJ, Buchanan CR, Valdés Hernández MC, Corley J, et al. Three major dimensions of human brain cortical ageing in relation to cognitive decline across the eighth decade of life. Mol Psychiatry 2021;26(6):2651–62. https://doi.org/10.1038/s41380-020-00975-1.
[8] de Frias CM, Lövdén M, Lindenberger U, Nilsson L-G. Revisiting the dedifferentiation hypothesis with longitudinal multi-cohort data. Intelligence 2007;35:381–92. https://doi.org/10.1016/j.intell.2006.07.011.
[9] Düzel S, Voelkle MC, Düzel E, Gerstorf D, Drewelies J, Steinhagen- Thiessen E, et al. The Subjective Health Horizon Questionnaire (SHH-Q): Assessing the future time perspectives for facets of an active lifestyle. Gerontology 2016;62(3):345–53. https://doi.org/10.1159/000441493.
[10] Edwards LJ, Kirilina E, Mohammadi S, Weiskopf N. Microstructural imaging of human neocortex in vivo. Neuroimage 2018;182:184–206. https://doi.org/10.1016/j.neuroimage.2018.02.055.
[11] Eid M, Nussbeck FW, Geiser C, Cole DA, Gollwitzer M, Lischetzke T. Structural equation modeling of multitrait-multimethod data: Different models for different types of methods. Psychol Methods 2008;13(3):230–53. https://doi.org/10.1037/a0013219.
[12] Ficiarà E, Stura I-A-O, Guiot C-A-O. Iron deposition in brain: Does aging matter? Int J Mol Sci 2022;23(17):10018. https://doi.org/10.3390/ijms231710018.
[13] Gorbach T, Pudas S, Bartrés-Faz D, Brandmaier AM, Düzel S, Henson RN, et al. Longitudinal association between hippocampus atrophy and episodic-memory decline in non-demented APOE-ε4 carriers. Alzheimers Dement 2020;12(1):e12110. https://doi.org/10.1002/dad2.12110.
[14] Gorbach T, Pudas S, Lundquist A, Orädd G, Josefsson M, Salami A, et al. Longitudinal association between hippocampus atrophy and episodic-memory decline. Neurobiol Aging 2017;51:167–76. https://doi.org/10.1016/j.neurobiolaging.2016.12.002.
[15] Grydeland H, Walhovd KB, Tamnes CK, Westlye LT, Fjell AM. Intracortical myelin links with performance variability across the human lifespan: Results from T1- and T2-weighted MRI myelin mapping and diffusion tensor imaging. J Neurosci 2013;33(47):18618–30. https://doi.org/10.1523/JNEUROSCI.2811-13.2013.
[16] Hertzog C. An individual differences perspective: Implications for cognitive research in gerontology. Res Aging 1985;7(1):7–45. https://doi.org/10.1177/0164027585007001002.
[17] Hof PR, Morrison JH. The aging brain: Morphomolecular senescence of cortical circuits. Trends Neurosci 2004;27(10):607–13. https://doi.org/10.1016/j.tins.2004.07.013.
[18] Jenkinson M, Beckmann CF, Behrens TE, Woolrich MW, Smith SM. FSL. Neuroimage 2012;62(2):782–90. https://doi.org/10.1016/j.neuroimage.2011.09.015.

[19] Johansson J, Wåhlin A, Lundquist A, Brandmaier AM, Lindenberger U, Nyberg L. Model of brain maintenance reveals specific change-change association between medial-temporal lobe integrity and episodic memory. Aging Brain 2022;10(2):100027. https://doi.org/10.1016/j.nbas.2021.100027.
[20] Köhncke Y, Düzel S, Sander MC, Lindenberger U, Kühn S, Brandmaier AM. Hippocampal and parahippocampal gray matter structural integrity assessed by multimodal imaging is associated with episodic memory in old age. Cereb Cortex 2021;31(3):1464–77. https://doi.org/10.1093/cercor/bhaa287.
[21] Kühn S, Düzel S, Eibich P, Krekel C, Wustemann H, Kolbe J, et al. In search of features that constitute an "enriched environment" in humans: Associations between geographical properties and brain structure. Sci Rep 2017;7(1):11920. https://doi.org/10.1038/s41598-017-12046-7.
[22] Lerch JP, van der Kouwe AJ, Raznahan A, Paus T, Johansen-Berg H, Miller KL, et al. Studying neuroanatomy using MRI. Nat Neurosci 2017;20(3):314–26. https://doi.org/10.1038/nn.4501.
[23] Lindenberger, U. (2020). *Human cognitive aging: Maintenance versus dedifferentiation*. Paper presented at the International Winter Conference on Brain-Computer Interface (BCI), Gangwon, Korea (South), Korea (South). https://ieeexplore.ieee.org/document/9061660.
[24] Lindenberger U, von Oertzen T, Ghisletta P, Hertzog C. Cross-sectional age variance extraction: What's change got to do with it? Psychol Aging 2011;26(1):34–47. https://doi.org/10.1037/a0020525.
[25] Morrison JH, Baxter MG. Synaptic health. *JAMA*. Psychiatry 2014;71(7):835–7. https://doi.org/10.1001/jamapsychiatry.2014.380.
[26] Nyberg L, Andersson M, Lundquist A, Baare WFC, Bartres-Faz D, Bertram L, et al. Individual differences in brain aging: Heterogeneity in cortico-hippocampal but not caudate atrophy rates. Cereb Cortex 2023;33(9):5075–81. https://doi.org/10.1093/cercor/bhac400.
[27] Nyberg L, Lindenberger U. Brain maintenance and cognition in old age. In: Poeppel D, Mangun G, Gazzaniga MS, editors. The cognitive neurosciences. 6th ed. Cambridge: MIT Press; 2020. p. 81–9.
[28] Nyberg L, Lövden M, Riklund K, Lindenberger U, Bäckman L. Memory aging and brain maintenance. Trends Cogn Sci 2012;16(5):292–305. https://doi.org/10.1016/j.tics.2012.04.005.
[29] Nyberg L, Pudas S. Successful memory aging. Annu Rev Psychol 2019;70(1):219–43. https://doi.org/10.1146/annurev-psych-010418-103052.
[30] Persson J, Stening E, Nordin K, Soderlund H. Predicting episodic and spatial memory performance from hippocampal resting-state functional connectivity: Evidence for an anterior-posterior division of function. Hippocampus 2018;28(1):53–66. https://doi.org/10.1002/hipo.22807.
[31] Pierpaoli C, Basser PJ. Toward a quantitative assessment of diffusion anisotropy. Magn Reson Med 1996;36(6):893–906. https://doi.org/10.1002/mrm.1910360612.
[32] Pudas S, Persson J, Josefsson M, de Luna X, Nilsson L-G, Nyberg L. Brain characteristics of individuals resisting age-related cognitive decline over two decades. J Neurosci 2013;33(20):8668–77. https://doi.org/10.1523/JNEUROSCI.2900-12.2013.
[33] Raz N, Daugherty AM. Pathways to brain aging and their modifiers: Free-Radical-Induced Energetic and Neural Decline in Senescence (FRIENDS) Model – A mini-review. Gerontology 2018;64(1):49–57. https://doi.org/10.1159/000479508.
[34] Raz N, Lindenberger U. Only time will tell: Cross-sectional studies offer no solution to the age–brain–cognition triangle: Comment on Salthouse (2011). Psychol Bull 2011;137(5):790–5. https://doi.org/10.1037/a0024503.
[35] Raz N, Lindenberger U, Rodrigue KM, Kennedy KM, Head D, Williamson A, et al. Regional brain changes in aging healthy adults: General trends, individual differences and modifiers. Cereb Cortex 2005;15(11):1676–89. https://doi.org/10.1093/cercor/bhi044.
[36] R Core Team.. *R: A language and environment for statistical computing*. Vienna, Austria: R Foundation for Statistical Computing; 2022.
[37] Rosseel Y. lavaan: An R package for structural equation modeling. J Stat Softw 2012;48(2):1–36. https://doi.org/10.18637/jss.v048.i02.
[38] Rubin DB. Inference and missing data. Biometrika 1976;63(3):581–92. https://doi.org/10.2307/2335739.
[39] Schafer JL, Graham JW. Missing data: Our view of the state of the art. Psychol Methods 2002;7(2):147–77. https://doi.org/10.1037/1082-989X.7.2.147.
[40] Schaie KW, Maitland SB, Willis SL, Intieri RC. Longitudinal invariance of adult psychometric ability factor structures across 7 years. Psychol Aging 1998;13:8–20. https://doi.org/10.1037/0882-7974.13.1.8.
[41] Schermelleh-Engel K, Kerwer M, Klein AG. Evaluation of model fit in nonlinear multilevel structural equation modeling. Front Psychol 2014;5:181. https://doi.org/10.3389/fpsyg.2014.00181.
[42] Seiler S, Pirpamer L, Hofer E, Duering M, Jouvent E, Fazekas F, et al. Magnetization transfer ratio relates to cognitive impairment in normal elderly. Front Aging Neurosci 2014;6:263. https://doi.org/10.3389/fnagi.2014.00263.
[43] Seiler S, Ropele S, Schmidt R. Magnetization transfer imaging for in vivo detection of microstructural tissue changes in aging and dementia: A short literature review. J Alzheimers Dis 2014;42(Suppl 3):S229–37. https://doi.org/10.3233/JAD-132750.
[44] Smith SM, Jenkinson M, Woolrich MW, Beckmann CF, Behrens TE, Johansen-Berg H, et al. Advances in functional and structural MR image analysis and implementation as FSL. Neuroimage 2004;23(Suppl 1):S208–19. https://doi.org/10.1016/j.neuroimage.2004.07.051.
[45] Sundgren PC, Dong Q, Gomez-Hassan D, Mukherji SK, Maly P, Welsh R. Diffusion tensor imaging of the brain: Review of clinical applications. Neuroradiology 2004;46(5):339–50. https://doi.org/10.1007/s00234-003-1114-x.
[46] Tucker-Drob EM, de la Fuente J, Köhncke Y, Brandmaier AM, Nyberg L, Lindenberger U. A strong dependency between changes in fluid and crystallized abilities in human cognitive aging. Sci Adv 2022;8(5):eabj2422. https://doi.org/10.1126/sciadv.abj2422.
[47] Tzourio-Mazoyer N, Landeau B, Papathanassiou D, Crivello F, Etard O, Delcroix N, et al. Automated anatomical labeling of activations in SPM using a macroscopic anatomical parcellation of the MNI MRI single-subject brain. Neuroimage 2002;15(1):273–89. https://doi.org/10.1006/nimg.2001.0978.
[48] Vidal-Pineiro D, Wang Y, Krogsrud SK, Amlien IK, Baaré WFC, Bartres-Faz D, et al. Individual variations in 'brain age' relate to early-life factors more than to longitudinal brain change. Elife 2021;10(10):e69995. https://doi.org/10.7554/eLife.69995.
[49] Walhovd KB, Lövden M, Fjell AM. Timing of lifespan influences on brain and cognition. Trends Cogn Sci 2023;27(10):P901–15. https://doi.org/10.1016/j.tics.2023.07.001.
[50] Walhovd KB, Nyberg L, Lindenberger U, Amlien IK, Sorensen O, Wang Y, et al. Brain aging differs with cognitive ability regardless of education. Sci Rep 2022;12(1):13886. https://doi.org/10.1038/s41598-022-17727-6.
[51] Weiskopf N, Edwards LJ, Helms G, Mohammadi S, Kirilina E. Quantitative magnetic resonance imaging of brain anatomy and in vivo histology. Nat Rev Phys 2021;3(8):570–88. https://doi.org/10.1038/s42254-021-00326-1.
[52] Wenger E, Polk SE, Kleemeyer MM, Weiskopf N, Bodammer NC, Lindenberger U, et al. Reliability of quantitative multiparameter maps is high for magnetization transfer and proton density but attenuated for R1 and R2* in healthy young adults. Hum Brain Mapp 2022;43(11):3585–603. https://doi.org/10.1002/hbm.25870.
[53] Wolff SD, Balaban RS. Magnetization transfer contrast (MTC) and tissue water proton relaxation in vivo. Magn Reson Med 1989;10(1):135–44. https://doi.org/10.1002/mrm.1910100113.